International Journal of Mechanical, Industrial and Aerospace Sciences
ISSN: 2517-9950
Vol:3, No:3, 2009

A Meshfree Solution of Tow-Dimensional Potential Flow Problems

I. V. Singh and A. Singh

***Abstract*—**In this paper, mesh-free element free Galerkin (EFG) method is extended to solve two-dimensional potential flow problems. Two ideal fluid flow problems (i.e. flow over a rigid cylinder and flow over a sphere) have been formulated using variational approach. Penalty and Lagrange multiplier techniques have been utilized for the enforcement of essential boundary conditions. Four point Gauss quadrature have been used for the integration on two-dimensional domain (Ω) and nodal integration scheme has been used to enforce the essential boundary conditions on the edges (Γ). The results obtained by EFG method are compared with those obtained by finite element method. The effects of scaling and penalty parameters on EFG results have also been discussed in detail.

***Keywords*—**Meshless, EFG method; potential flow, Lagrange multiplier method; penalty method; penalty parameter and scaling parameter.

I. Introduction

NOW a day, a number of numerical tools are available to solve fluid flow problems including finite difference method (FDM), finite volume method (FVM) and finite element method (FEM). But the numerical simulation of fluid flow problems in complex geometries still remains a challenging task for the researchers and scientists. Even with availability of powerful mesh generators, the time required in mesh generation process for complex geometries is quite large in comparison to the solution and often leads to numerical errors. Therefore, to overcome these problems, a number of numerical methods were proposed in past few years. In these methods, the requirement of meshes is totally unnecessary. The essential feature of these methods is that they only require a set of nodes to construct the approximation function. These methods are named as mesh-free or meshless methods. For more than ten years, the meshless methods were successfully applied in different areas of engineering and science including fluid flow problems. Lin and Atluri [1], [2] used meshless local Petrov Galerkin method (MLPG) to solve Navier-Strokes equation for incompressible fluids and convection-diffusion equation for flow problems. Mesh-free finite point method is utilized to solve advective–diffusive transport and fluid mechanics problem by Oňate and his co-workers [3], [4]. The further use of finite point method has been done by Löhner *et al*. [5] to solve compressible flow problem. Sophy and Sadat [6] have solved three dimensional laminar natural convection problems by diffuse approximation method. Liu *et al.* [7] used reproducing kernel particle method to solve fluid dynamics problem in which they introduced the multiple scale adaptive refinement technique. A radial basis function based meshless method has been used by Han and Huang [8] to model the shear flow of Johnson-Segalman fluid. Tsukanov *et al.* [9] used R-function method for the solution of incompressible fluid dynamics problems. Some of these meshless methods have also been extended to solve potential flow problems. Chen and Raju [10] used coupled finite element and MLPG method to solve two-dimensional potential flow problems. Novel finite point method has been used by Cheng and Liu [11] to analyze the flow around a cylinder**.**

In recent years, the meshless element free Galerkin (EFG) method has been extensively used to solve a variety of problems in different areas of engineering and science including fluid flow. Singh [12] used the EFG method to solve viscous incompressible fluid flow problems. Du [13] used this method for the simulation of stationary two-dimensional shallow flows in rivers, and Verardi *et al.* [14] applied this method for the study of fully developed magnetohydrodynamic duct flows.

In the present work, the EFG method has been extended to solve two-dimensional potential flow problems. Two ideal fluid flow problems i.e. flow over a rigid cylinder kept between two parallel plates and flow over a sphere kept inside a cylinder have been chosen and solved using penalty as well as Lagrange multiplier techniques. Nodal integration approach has been utilized to enforce the essential boundary conditions along the edges of the 2-D computational domain and Gaussian quadrature approach has been used to integrate over computational domain. The EFG results have been obtained for two model fluid flow problems, and are compared with those obtained by finite element method. The effect of scaling as well as penalty parameter has also been discussed in detail.

Manuscript received January 7, 2008.

I. V. Singh is with the Department of Mechanical and Industrial Engineering, Indian Institute of Technology-Roorkee, Uttaranchal, India (phone: +91-1332-285888, fax: +91-1332-285665, e-mail: indrafme@iitr.ernet.in).

A. Singh is with the Department of Mechanical Engineering, Birla Institute of Technology and Science, Pilani, Rajasthan, India phone: +91-1596-242703, e-mail: akhilendra.singh@gmail.com)

II. Overview of EFG method

A. MLS Approximation

The of the governing equations by element free Galerkin (EFG) method requires moving least square (MLS) interpolation functions which are made up of three components: a weight function associated with each node, a basis function and a set of non-constant coefficients. The weight function is non-zero over a small neighborhood at a particular node, called support of the node. Using MLS approximation, the unknown stream function $\Psi(x, y)$ is approximated by $\Psi^h(x, y)$ over the two-dimensional domain [15].

$$\Psi(x, y) \approx \Psi^h(x, y) = \sum_{j=1}^{m} p_j(x,y)\, a_j(x,y) \equiv \mathbf{p}^T(\mathbf{x})\,\mathbf{a}(\mathbf{x}) \tag{1}$$

Where, m = number of terms in the basis, $p_j(x,y)$ = monomial basis function, $a_j(x,y)$ =non-constant coefficients: $\mathbf{x}^T = [x \quad y]$, $\mathbf{p}^T(\mathbf{x}) = [1 \quad x \quad y]$. The coefficients $a_j(\mathbf{x})$ are determined by minimizing the functional $J(\mathbf{x})$ given by

$$J(\mathbf{x}) = \sum_{I=1}^{n} w(\mathbf{x}-\mathbf{x}_I)\left\{\sum_{j=1}^{m} p_j(\mathbf{x}_I)\, a_j(\mathbf{x}) - \Psi_{\mathbf{I}}\right\}^2 \tag{2}$$

Where, $w(\mathbf{x}-\mathbf{x}_I)$ is a weight function which is non zero over a small domain, called domain of influence, n is the number of nodes in the domain of influence. The minimization of $J(\mathbf{x})$ w.r.to $\mathbf{a}(\mathbf{x})$ leads to the following set of equations

$$\mathbf{a}(\mathbf{x}) = \mathbf{C}^{-1}(\mathbf{x})\,\mathbf{D}(\mathbf{x})\,\boldsymbol{\Psi} \tag{3}$$

Where, $\mathbf{C}$ and $\mathbf{D}$ are given as

$$\mathbf{C} = \sum_{I=1}^{n} w(\mathbf{x}-\mathbf{x}_I)\,\mathbf{p}(\mathbf{x}_I)\,\mathbf{p}^T(\mathbf{x}_I) \tag{4}$$

$$\mathbf{D}(\mathbf{x}) = [w(\mathbf{x}-\mathbf{x}_1)\mathbf{p}(\mathbf{x}_1), w(\mathbf{x}-\mathbf{x}_2)\mathbf{p}(\mathbf{x}_2), ..., w(\mathbf{x}-\mathbf{x}_n)\mathbf{p}(\mathbf{x}_n)] \tag{5}$$

$$\boldsymbol{\Psi}^T = [\Psi_1, \Psi_2, \Psi_3 ..., \Psi_n] \tag{6}$$

By substituting Eq. (3) in Eq. (1), the MLS approximants can be defined as

$$\Psi^h(\mathbf{x}) = \sum_{I=1}^{n} \Phi_I(\mathbf{x})\,\Psi_I = \boldsymbol{\Phi}(\mathbf{x})\boldsymbol{\Psi} \tag{7}$$

Where, the shape function $\Phi_I(\mathbf{x})$ is defined by

$$\Phi_I(\mathbf{x}) = \sum_{j=1}^{m} p_j(\mathbf{x})(\mathbf{C}^{-1}(\mathbf{x})\mathbf{D}(\mathbf{x}))_{jI} = \mathbf{p}^T\mathbf{C}^{-1}\mathbf{D}_I \tag{8}$$

B. The Weight Function

The weight function is non-zero over a small neighborhood of $\mathbf{x}_I$, called the domain of influence of node I. The choice of weight function $w(\mathbf{x}-\mathbf{x}_I)$ affects the resulting approximation $\Psi^h(\mathbf{x}_I)$. In the present work, cubicspline weight function [15] has been used due to its accuracy, which can be written as a function of normalized radius $\bar{r}$ as

$$w(\bar{r}) = \begin{cases} 2/3 - 4\bar{r}^2 + 4\bar{r}^3 & \text{for } \bar{r} \le 1/2 \\ 4/3 - 4\bar{r} + 4\bar{r}^2 - (4/3)\bar{r}^3 & \text{for } 1/2 < \bar{r} \le 1 \\ 0 & \text{for } \bar{r} > 1 \end{cases} \tag{9}$$

With $\bar{r}_I = \|\mathbf{x}-\mathbf{x}_I\|/d_{mI}$, $\bar{r}_{xI} = \| x - x_I \| / d_{mxI}$, $\bar{r}_{yI} = \| y - y_I \| / d_{myI}$, $d_{mxI} = d_{\max} c_{xI}$, $d_{myI} = d_{\max} c_{yI}$ and $d_{\max}$ is a scaling parameter and c_{xI} & c_{yI} at node I, are the distances to the nearest neighbors. The weight function at any given point can be calculated as

$$w(\mathbf{x}-\mathbf{x}_I) = w(\bar{r}_x)\, w(\bar{r}_y) = w_x\, w_y \tag{10}$$

Where, $w(\bar{r}_x)$ or $w(\bar{r}_y)$ can be calculated by replacing $\bar{r}$ by $\bar{r}_x$ or $\bar{r}_y$ in the expression of $w(\bar{r})$.

III. The flow over a rigid cylinder

A. Variational Formulation

Consider two-dimensional potential flow of an ideal (inviscid incompressible) fluid over a rigid cylinder, which is kept between two parallel plates, is given by Laplace equation

$$\nabla^2\Psi \equiv \frac{\partial^2\Psi}{\partial x^2} + \frac{\partial^2\Psi}{\partial y^2} = 0 \tag{11a}$$

$$\left.\begin{array}{ll} \text{at the edge, } \Gamma_l & \Psi = \Psi_1(y) \\ \text{at the edge, } \Gamma_b & \Psi = \Psi_2 \\ \text{at the edge, } \Gamma_{arc} & \Psi = \Psi_3 \\ \text{at the edge, } \Gamma_{rt} & \dfrac{\partial\Psi}{\partial x} = 0 \\ \text{at the edge, } \Gamma_t & \Psi = \Psi_4 \end{array}\right\} \tag{11b}$$

The weighted integral form of Eq. (11a) is obtained as

$$\int_{\Omega} w_1 \left\{\frac{\partial^2\Psi}{\partial x^2} + \frac{\partial^2\Psi}{\partial y^2}\right\} d\Omega = 0 \tag{12}$$

The weak form of Eq. (12) is given by

$$-\int_{\Omega}\left[\frac{\partial w_1}{\partial x}\frac{\partial\Psi}{\partial x} + \frac{\partial w_1}{\partial y}\frac{\partial\Psi}{\partial y}\right] d\Omega + \int_{\Gamma} w_1 \left\{\frac{\partial\Psi}{\partial x} + \frac{\partial\Psi}{\partial y}\right\} d\Gamma = 0 \tag{13}$$

Using natural boundary conditions, the functional $I(\Psi)$ is obtained as

$$I(\Psi) = \frac{1}{2}\int_{\Omega}\left[\left(\frac{\partial\Psi}{\partial x}\right)^2 + \left(\frac{\partial\Psi}{\partial y}\right)^2\right] d\Omega \tag{14}$$

B. Enforcement of Essential Boundary Conditions

In this work, Lagrange multiplier and penalty methods have been used for the enforcement of essential boundary conditions. Lagrange multiplier method (LMM) is chosen due to its accuracy and penalty method is used due to its simplicity.

Lagrange multiplier method (LMM)

Using Lagrange multiplier method (LMM) to enforce essential

boundary conditions, the functional $I^*(\Psi)$ is obtained as

$$I^*(\Psi)=\frac{1}{2}\int_\Omega\left[\left(\frac{\partial\Psi}{\partial x}\right)^2+\left(\frac{\partial\Psi}{\partial y}\right)^2\right]d\Omega+\int_{\Gamma_l}\lambda_1\{\Psi-\Psi_1(y)\}d\Gamma + \int_{\Gamma_b}\lambda_2\{\Psi-\Psi_2\}d\Gamma+\int_{\Gamma_{arc}}\lambda_3\{\Psi-\Psi_3\}d\Gamma+\int_{\Gamma_t}\lambda_4\{\Psi-\Psi_4\}d\Gamma \quad (15)$$

Taking variation i.e. $\delta I^*(\Psi)$ of Eq. (15), it reduces to

$$\delta I^*(\Psi)=\int_\Omega\left[\left(\frac{\partial\Psi}{\partial x}\right)^T\delta\left(\frac{\partial\Psi}{\partial x}\right)+\left(\frac{\partial\Psi}{\partial y}\right)^T\delta\left(\frac{\partial\Psi}{\partial y}\right)\right]d\Omega+ \int_{\Gamma_b}\left[\delta\lambda_2\{\Psi-\Psi_2\}+\lambda_2\delta\Psi\right]d\Gamma+\int_{\Gamma_l}\left[\delta\lambda_1\{\Psi-\Psi_1(y)\}+\lambda_1\delta\Psi\right]d\Gamma+ \int_{\Gamma_{arc}}\left[\delta\lambda_3\{\Psi-\Psi_3\}+\lambda_3\delta\Psi\right]d\Gamma+\int_{\Gamma_t}\left[\delta\lambda_4\{\Psi-\Psi_4\}+\lambda_4\delta\Psi\right]d\Gamma \quad (16)$$

Since $\delta I^*(\Psi)=0$ and $\delta\Psi$, $\delta\lambda_1$, $\delta\lambda_2$, $\delta\lambda_3$ & $\delta\lambda_4$ are arbitrary in Eq. (16), a following set of equations is obtained using Eq. (7)

$$\begin{bmatrix}\mathbf{K} & \mathbf{G}1 & \mathbf{G}2 & \mathbf{G}3 & \mathbf{G}4\\ \mathbf{G}1^T & 0 & 0 & 0 & 0\\ \mathbf{G}2^T & 0 & 0 & 0 & 0\\ \mathbf{G}3^T & 0 & 0 & 0 & 0\\ \mathbf{G}4^T & 0 & 0 & 0 & 0\end{bmatrix}\begin{Bmatrix}\boldsymbol{\Psi}\\ \boldsymbol{\lambda}1\\ \boldsymbol{\lambda}2\\ \boldsymbol{\lambda}3\\ \boldsymbol{\lambda}4\end{Bmatrix}=\begin{Bmatrix}\mathbf{f}\\ \mathbf{q1}\\ \mathbf{q2}\\ \mathbf{q3}\\ \mathbf{q4}\end{Bmatrix} \quad (17)$$

Where,

$$K_{IJ}=\int_\Omega\left\{\Phi_{I,x}^T\Phi_{J,x}+\Phi_{I,y}^T\Phi_{J,y}\right\}d\Omega \quad (18a)$$

$$f_I=0 \quad (18b)$$

$$G1_{IK}=\int_{\Gamma_l}\Phi_I N_K d\Gamma \quad (18c)$$

$$G2_{IK}=\int_{\Gamma_b}\Phi_I N_K d\Gamma \quad (18d)$$

$$G3_{IK}=\int_{\Gamma_{arc}}\Phi_I N_K d\Gamma \quad (18e)$$

$$G4_{IK}=\int_{\Gamma_t}\Phi_I N_K d\Gamma \quad (18f)$$

$$q1_K=\int_{\Gamma_l}\Psi_1(y)N_K d\Gamma \quad (18g)$$

$$q2_K=\int_{\Gamma_b}\Psi_2 N_K d\Gamma \quad (18h)$$

$$q3_K=\int_{\Gamma_{arc}}\Psi_3 N_K d\Gamma \quad (18i)$$

$$q4_K=\int_{\Gamma_t}\Psi_4 N_K d\Gamma \quad (18j)$$

Penalty method (PM)

Using penalty method (PM) to enforce essential boundary conditions, the functional $I^*(\Psi)$ is obtained as

$$I^*(\Psi)=\frac{1}{2}\int_\Omega\left[\left(\frac{\partial\Psi}{\partial x}\right)^2+\left(\frac{\partial\Psi}{\partial y}\right)^2\right]d\Omega+\int_{\Gamma_l}\frac{\alpha}{2}\{\Psi-\Psi_1(y)\}^2\,d\Gamma+ \int_{\Gamma_b}\frac{\alpha}{2}\{\Psi-\Psi_2\}^2\,d\Gamma+\int_{\Gamma_{arc}}\frac{\alpha}{2}\{\Psi-\Psi_3\}^2\,d\Gamma+\int_{\Gamma_t}\frac{\alpha}{2}\{\Psi-\Psi_4\}^2\,d\Gamma \quad (19)$$

Taking variation i.e. $\delta I^*(\Psi)$ of Eq. (19), it reduces to

$$\delta I^*(\Psi)=\int_\Omega\left[\left(\frac{\partial\Psi}{\partial x}\right)^T\delta\left(\frac{\partial\Psi}{\partial x}\right)+\left(\frac{\partial\Psi}{\partial y}\right)^T\delta\left(\frac{\partial\Psi}{\partial y}\right)\right]d\Omega+ \int_{\Gamma_b}\alpha\{\Psi-\Psi_2\}\delta\Psi d\Gamma+\int_{\Gamma_{arc}}\alpha\{\Psi-\Psi_3\}\delta\Psi d\Gamma+ \int_{\Gamma_l}\alpha\{\Psi-\Psi_1(y)\}\delta\Psi d\Gamma+\int_{\Gamma_t}\alpha\{\Psi-\Psi_4\}\delta\Psi d\Gamma \quad (20)$$

Since $\delta I^*(\Psi)=0$ and $\delta\Psi$ are arbitrary in Eq. (20), a following set of equations is obtained using Eq. (7)

$$[\mathbf{K}]\{\boldsymbol{\Psi}\}=\{\mathbf{f}\} \quad (21)$$

$$K_{IJ}=\int_\Omega\left\{\Phi_{I,x}^T\Phi_{J,x}+\Phi_{I,y}^T\Phi_{J,y}\right\}d\Omega+\alpha\int_{\Gamma_l}\Phi_I{}^T\Phi_J d\Gamma+ \alpha\int_{\Gamma_b}\Phi_I{}^T\Phi_J d\Gamma+\alpha\int_{\Gamma_{arc}}\Phi_I{}^T\Phi_J d\Gamma+\alpha\int_{\Gamma_t}\Phi_I{}^T\Phi_J d\Gamma \quad (22a)$$

$$f_I=\alpha\int_{\Gamma_l}\Psi_1(y)\Phi_I d\Gamma+\alpha\int_{\Gamma_b}\Psi_2\Phi_I d\Gamma+ \alpha\int_{\Gamma_{arc}}\Psi_2\Phi_I d\Gamma+\alpha\int_{\Gamma_b}\Psi_2\Phi_I d\Gamma \quad (22b)$$

IV. AXISYMMETRIC FLOW

A. Variational Formulation

Consider the flow of an ideal fluid over a sphere, which is kept inside a cylinder. This problem is modeled as an axisymmetric two-dimensional potential flow problem and the governing Laplacian equation in cylindrical coordinate system reduces to Stokesian equation given by

$$\nabla^2(\Psi)\equiv\frac{\partial^2\Psi}{\partial z^2}+\frac{\partial^2\Psi}{\partial r^2}-\frac{1}{r}\frac{\partial\Psi}{\partial r}=0 \quad (23a)$$

with the following essential and natural boundary conditions

$$\left.\begin{array}{ll}\text{at the edge, } \Gamma_l & \Psi_1(r)=u_o\,r\\ \text{at the edge, } \Gamma_b & \Psi_2=0\\ \text{at the edge, } \Gamma_{arc} & \Psi_3=0\\ \text{at the edge, } \Gamma_{rt} & \dfrac{\partial\Psi}{\partial z}=0\\ \text{at the edge, } \Gamma_t & \Psi_4=u_o\,H\end{array}\right\} \quad (23b)$$

The weighted integral form of Eq. (23a) is obtained as

$$2\pi \int_{\Omega} w_1 \left\{ \frac{\partial^2 \Psi}{\partial z^2} + \frac{\partial^2 \Psi}{\partial r^2} - \frac{1}{r}\frac{\partial \Psi}{\partial r} \right\} r\, dr\, dz = 0 \tag{24}$$

The weak form of Eq. (24) is given by

$$\begin{aligned} &-2\pi \int_{\Omega} \left[\frac{\partial w_1}{\partial z}\frac{\partial \Psi}{\partial z} + \frac{\partial w_1}{\partial r}\frac{\partial \Psi}{\partial r} + \frac{2w_1}{r}\frac{\partial \Psi}{\partial r} \right] r\, dr\, dz + \\ &2\pi \int_{\Gamma} w_1 r \left\{ \frac{\partial \Psi}{\partial z} n_z + \frac{\partial \Psi}{\partial r} n_r \right\} d\Gamma = 0 \end{aligned} \tag{25}$$

Where, n_r and n_z are the direction cosines of the outward normal to the respective edges.

Using natural boundary conditions, the functional $I(\Psi)$ is obtained as

$$I(\Psi) = \pi \int_{\Omega} \left[\left(\frac{\partial \Psi}{\partial z} \right)^2 + \left(\frac{\partial \Psi}{\partial r} \right)^2 + \frac{2\Psi}{r}\frac{\partial \Psi}{\partial r} \right] r\, dr\, dz \tag{26}$$

B. Enforcement of Essential Boundary Conditions

Both Lagrange multiplier and penalty methods have been used for the enforcement of essential boundary conditions.

Lagrange multiplier method (LMM)

Using Lagrange multiplier method (LMM) to enforce essential boundary conditions, the functional $I^*(\Psi)$ is obtained as

$$\begin{aligned} I^*(\Psi) = \pi \int_{\Omega} &\left[\left(\frac{\partial \Psi}{\partial z} \right)^2 + \left(\frac{\partial \Psi}{\partial r} \right)^2 + \frac{2\Psi}{r}\frac{\partial \Psi}{\partial r} \right] r\, dr\, dz + \\ &\int_{\Gamma_l} \lambda_1 \{\Psi - \Psi_1(r)\} d\Gamma + \int_{\Gamma_b} \lambda_2 \{\Psi - \Psi_2\}\, d\Gamma + \\ &\int_{\Gamma_{arc}} \lambda_3 \{\Psi - \Psi_3\}\, d\Gamma + \int_{\Gamma_t} \lambda_4 \{\Psi - \Psi_4\} d\Gamma \end{aligned} \tag{27}$$

Taking variation i.e. $\delta I^*(\Psi)$ of Eq. (27), it reduces to

$$\begin{aligned} \delta I^*(\Psi) = &2\pi \int_{\Omega} \left[r\left(\frac{\partial \Psi}{\partial z} \right)^T \delta\left(\frac{\partial \Psi}{\partial z} \right) + r\left(\frac{\partial \Psi}{\partial r} \right)^T \left(\frac{\partial \Psi}{\partial r} \right) \right] dr\, dz \\ &+ 2\pi \int_{\Omega} \left[\Psi^T \delta\left(\frac{\partial \Psi}{\partial r} \right) + \left(\frac{\partial \Psi}{\partial r} \right)^T \delta\Psi \right] dr\, dz \\ &+ \int_{\Gamma_l} \left[\delta\lambda_1 \{\Psi - \Psi_1(r)\} + \lambda_1 \delta\Psi \right] d\Gamma + \int_{\Gamma_b} \left[\delta\lambda_2 \{\Psi - \Psi_2\} + \lambda_2 \delta\Psi \right] d\Gamma \\ &+ \int_{\Gamma_{arc}} \left[\delta\lambda_3 \{\Psi - \Psi_3\} + \lambda_3 \delta\Psi \right] d\Gamma + \int_{\Gamma_t} \left[\delta\lambda_4 \{\Psi - \Psi_4\} + \lambda_4 \delta\Psi \right] d\Gamma \end{aligned} \tag{28}$$

Since $\delta I^*(\Psi) = 0$ and $\delta\Psi$, $\delta\lambda_1$, $\delta\lambda_2$, $\delta\lambda_3$ & $\delta\lambda_4$ are arbitrary in Eq. (28), a following set of equations is obtained using Eq. (7)

$$\begin{bmatrix} \mathbf{K} & \mathbf{G}1 & \mathbf{G}2 & \mathbf{G}3 & \mathbf{G}4 \\ \mathbf{G}1^T & 0 & 0 & 0 & 0 \\ \mathbf{G}2^T & 0 & 0 & 0 & 0 \\ \mathbf{G}3^T & 0 & 0 & 0 & 0 \\ \mathbf{G}4^T & 0 & 0 & 0 & 0 \end{bmatrix} \begin{Bmatrix} \boldsymbol{\Psi} \\ \boldsymbol{\lambda}1 \\ \boldsymbol{\lambda}2 \\ \boldsymbol{\lambda}3 \\ \boldsymbol{\lambda}4 \end{Bmatrix} = \begin{Bmatrix} \mathbf{f} \\ \mathbf{q1} \\ \mathbf{q2} \\ \mathbf{q3} \\ \mathbf{q4} \end{Bmatrix} \tag{29}$$

where,

$$\begin{aligned} K_{IJ} = = &2\pi \int_{\Omega} r \left\{ \Phi_{I,z}^T \Phi_{J,z} + \Phi_{I,r}^T \Phi_{J,r} \right\} dr\, dz + \\ &2\pi \int_{\Omega} \left\{ \Phi_I^T \Phi_{J,r} + \Phi_{I,r}^T \Phi_J \right\} dr\, dz \end{aligned} \tag{30a}$$

$$f_I = 0 \tag{30b}$$

$$G1_{IK} = \int_{\Gamma_l} \Phi_I N_K d\Gamma \tag{30c}$$

$$G2_{IK} = \int_{\Gamma_b} \Phi_I N_K d\Gamma \tag{30d}$$

$$G3_{IK} = \int_{\Gamma_{arc}} \Phi_I N_K d\Gamma \tag{30e}$$

$$G4_{IK} = \int_{\Gamma_t} \Phi_I N_K d\Gamma \tag{30f}$$

$$q1_K = \int_{\Gamma_l} \Psi_1(y) N_K d\Gamma \tag{30g}$$

$$q2_K = \int_{\Gamma_b} \Psi_2 N_K d\Gamma \tag{30h}$$

$$q3_K = \int_{\Gamma_{arc}} \Psi_3 N_K d\Gamma \tag{30i}$$

$$q4_K = \int_{\Gamma_t} \Psi_4 N_K d\Gamma \tag{30j}$$

Penalty method (PM)

Using penalty method (PM) to enforce essential boundary conditions, the functional $I^*(\Psi)$ is obtained as

$$\begin{aligned} I^*(\Psi) = \pi \int_{\Omega} &\left[\left(\frac{\partial \Psi}{\partial z} \right)^2 + \left(\frac{\partial \Psi}{\partial r} \right)^2 + \frac{2\Psi}{r}\frac{\partial \Psi}{\partial r} \right] r\, dr\, dz + \\ &\int_{\Gamma_l} \frac{\alpha}{2} \{\Psi - \Psi_1(y)\}^2 d\Gamma + \int_{\Gamma_b} \frac{\alpha}{2} \{\Psi - \Psi_2\}^2 d\Gamma + \\ &\int_{\Gamma_{arc}} \frac{\alpha}{2} \{\Psi - \Psi_3\}^2 d\Gamma + \int_{\Gamma_t} \frac{\alpha}{2} \{\Psi - \Psi_4\}^2 d\Gamma \end{aligned} \tag{31}$$

Taking variation i.e. $\delta I^*(\Psi)$ of Eq. (31), it reduces to

$$\delta I^*(\Psi) = 2\pi \int_\Omega \left[r\left(\frac{\partial \Psi}{\partial z}\right)^T \delta\left(\frac{\partial \Psi}{\partial z}\right) + r\left(\frac{\partial \Psi}{\partial r}\right)^T \left(\frac{\partial \Psi}{\partial r}\right) \right] dr\,dz + 2\pi \int_\Omega \left[\Psi^T \delta\left(\frac{\partial \Psi}{\partial r}\right) + \left(\frac{\partial \Psi}{\partial r}\right)^T \delta\Psi \right] dr\,dz + \int_{\Gamma_l} \alpha\{\Psi - \Psi_1(y)\}\delta\Psi d\Gamma + \int_{\Gamma_b} \alpha\{\Psi - \Psi_2\}\delta\Psi d\Gamma + \int_{\Gamma_{arc}} \alpha\{\Psi - \Psi_3\}\delta\Psi d\Gamma + \int_{\Gamma_t} \alpha\{\Psi - \Psi_4\}\delta\Psi d\Gamma \quad (32)$$

Since $\delta I^*(\Psi) = 0$ and $\delta\Psi$ are arbitrary in Eq. (32), a following set of equations is obtained using Eq. (7)

$$[\mathbf{K}]\{\boldsymbol{\Psi}\} = \{\mathbf{f}\} \quad (33)$$

Where,

$$K_{IJ} = 2\pi \int_\Omega r\left\{\Phi_{I,z}^T \Phi_{J,z} + \Phi_{I,r}^T \Phi_{J,r}\right\} dr\,dz + 2\pi \int_\Omega \left\{\Phi_I{}^T \Phi_{J,r} + \Phi_{I,r}^T \Phi_J\right\} dr\,dz + \alpha \int_{\Gamma_l} \Phi_I{}^T \Phi_J d\Gamma + \alpha \int_{\Gamma_b} \Phi_I{}^T \Phi_J d\Gamma + \alpha \int_{\Gamma_{arc}} \Phi_I{}^T \Phi_J d\Gamma + \alpha \int_{\Gamma_t} \Phi_I{}^T \Phi_J d\Gamma \quad (34a)$$

$$f_I = \alpha \int_{\Gamma_l} \Psi_1(y)\Phi_I d\Gamma + \alpha \int_{\Gamma_b} \Psi_2 \Phi_I d\Gamma + \alpha \int_{\Gamma_{arc}} \Psi_3 \Phi_I d\Gamma + \alpha \int_{\Gamma_t} \Psi_4 \Phi_I d\Gamma \quad (34b)$$

V. Numerical Results and Discussion

Two problems i.e. (an ideal flow over a rigid cylinder kept between two parallel plates and an ideal flow over a sphere kept inside the cylinder) have been chosen for the solution of potential flow problems. The governing equation for the first problem is Laplacian equation and for the second one is Stokesian equation. Four point Gauss quadrature have been used to evaluate the integrals over two-dimensional domain and nodal integration technique is utilized to enforce the essential boundary conditions on the edges. The EFG results have obtained using linear basis & cubicspline weight function for two sets of nodes whereas FEM results (Chung 1978) have been obtained for the same sets of nodes.

A. Potential Flow over a Cylinder

The model, data and its boundary conditions used for the potential flow over a cylinder kept between two parallel plates are shown in Fig. 1. The EFG results have been obtained using Lagrange multiplier and penalty methods for two sets of nodes i.e. 55 and 128 nodes. Table 1 shows a comparison of stream function values (Ψ) obtained by EFG method with those obtained by FEM for 55 nodes at few typical locations. A similar comparison of EFG results with FEM results is presented in Table 2 at the same locations for 128 nodes. The maximum percentage difference in stream function values obtained by LMM is found to be 2.23% for 55 nodes and 0.26% for 128 nodes, whereas the maximum percentage difference in stream function values obtained by PM is found to be 2.23% for 55 nodes and 0.26% for 128 nodes. A comparison of velocity values (u) obtained by EFG method with FEM is presented in Table 3 and Table 4 for 55 and 128 nodes respectively at the few typical locations. The maximum percentage difference in velocity values obtained by LMM is found to be 7.67% for 55 nodes and 2.60% for 128 nodes, whereas the maximum percentage difference in velocity values obtained by PM has been found to be 7.24% for 55 nodes and 2.60% for 128 nodes. From the results presented in Tables 1─4, it can be concluded that the results obtained by LMM are almost similar to PM. Moreover, with the increase in number of nodes, the EFG results start conversing for both LMM and PM.

The effect of scaling parameter ($d_{\max}$) on EFG results has been presented in Fig. 2 at the location ($x = 2, y = 1$) for 55 and 128 nodes. A similar comparison of EFG results has been presented in Figs. 3, 4 and 5 at the locations ($x = 4, y = 1.5$), ($x = 2, y = 0.75$) and ($x = 4, y = 1.375$) respectively for the same set of sets. From the results presented in Figs. 2─5, it is observed that the scaling parameter gives acceptable results in the range 1.1─2 for both LMM and PM.

The effect of penalty parameter (α) on EFG results has been presented in Fig. 6 at the location ($x = 2, y = 1$) for 55 and 128 nodes. A similar comparison of EFG results has been presented in Figs. 7, 8 and 9 at the locations ($x = 4, y = 1.5$), ($x = 2, y = 0.75$) and ($x = 4, y = 1.375$) respectively for 55 and 128 nodes. From Figs. 7─9, it has been noticed that the acceptable range of penalty parameter varies from 10^3 to 10^{15}.

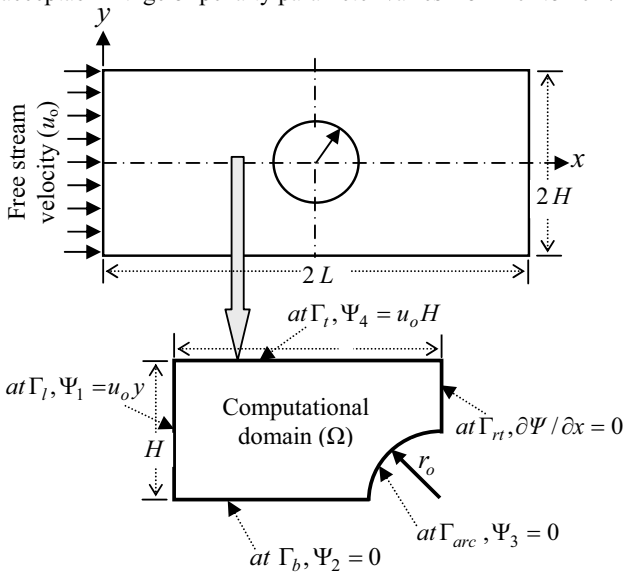

(L = 4 m, H = 2 m, r_o =1 m, u_o = 1m/s)

Fig. 1 Potential flow over a cylinder kept between two parallel plates

TABLE I COMPARISON OF STREAM FUNCTION (Ψ) WITH FEM FOR 55 NODES AT THE FEW TYPICAL LOCATIONS

Location		55 nodes				
		EFG				FEM
x	y	LMM	% diff	PM	% diff	
1.0	1.5	1.4907	0.25	1.4908	0.26	1.4870
1.5	1.5	1.4782	0.43	1.4782	0.43	1.4719
2.0	1.5	1.4504	0.57	1.4505	0.58	1.4422
3.0	1.5	1.2906	0.62	1.2907	0.63	1.2826
3.0	1.0	0.6266	1.97	0.6268	2.00	0.6145
4.0	1.75	1.5529	0.01	1.5528	0.01	1.5527
4.0	1.5	1.0969	0.98	1.0969	0.98	1.0863
4.0	1.25	0.5921	2.23	0.5921	2.23	0.5792

TABLE II COMPARISON OF STREAM FUNCTION (Ψ) WITH FEM FOR 128 NODES AT THE FEW TYPICAL LOCATIONS

Location		128 nodes				
		EFG				FEM
x	y	LMM	% diff	PM	% diff	
1.0	1.5	1.4897	0.17	1.4897	0.17	1.4872
1.5	1.5	1.4756	0.22	1.4756	0.22	1.4723
2.0	1.5	1.4459	0.23	1.4459	0.23	1.4426
3.0	1.5	1.2839	0.03	1.2839	0.03	1.2835
3.0	1.0	0.6092	0.08	0.6092	0.08	0.6087
4.0	1.75	1.5524	0.01	1.5524	0.01	1.5523
4.0	1.5	1.0889	0.13	1.0889	0.13	1.0875
4.0	1.25	0.5869	0.26	0.5869	0.26	0.5854

TABLE III COMPARISON OF VELOCITY (u) WITH FEM FOR 55 NODES AT THE FEW TYPICAL LOCATIONS

Location		55 nodes				
		EFG				FEM
x	y	LMM	% diff	PM	% diff	
1.5	1.75	1.0436	1.18	1.0436	1.18	1.5
1.5	0.75	0.9824	0.39	0.9822	0.37	1.5
3.0	1.25	1.3280	0.61	1.3278	0.63	3.0
3.0	0.75	0.8694	7.67	0.8734	7.24	3.0
4.0	1.875	1.7884	0.05	1.7884	0.05	4.0
4.0	1.625	1.8240	2.22	1.8236	2.24	4.0
4.0	1.375	2.0192	0.46	2.0192	0.46	4.0
4.0	1.125	2.3684	2.23	2.3684	2.23	4.0

TABLEIV COMPARISON OF VELOCITY (u) WITH FEM FOR 128 NODES AT THE FEW TYPICAL LOCATIONS

Location		128 nodes				
		EFG				FEM
x	y	LMM	% diff	PM	% diff	
1.5	1.75	1.0488	0.62	1.0488	0.62	1.0553
1.5	0.75	0.9834	0.33	0.9834	0.33	0.9802
3.0	1.25	1.3494	0.13	1.3494	0.13	1.3477
3.0	0.75	1.0144	2.60	1.0144	2.60	0.9887
4.0	1.875	1.7904	0.02	1.7904	0.02	1.7908
4.0	1.625	1.8540	0.27	1.8540	0.27	1.8591
4.0	1.375	2.0080	0.01	2.0080	0.01	2.0082
4.0	1.125	2.3476	0.25	2.3476	0.25	2.3418

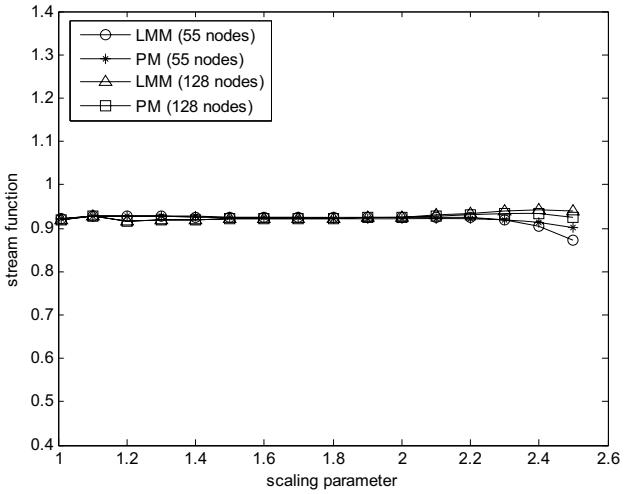

Fig. 2 Effect of scaling parameter on stream function (Ψ) at ($x = 2\ m, y = 1\ m$) for two sets of nodes

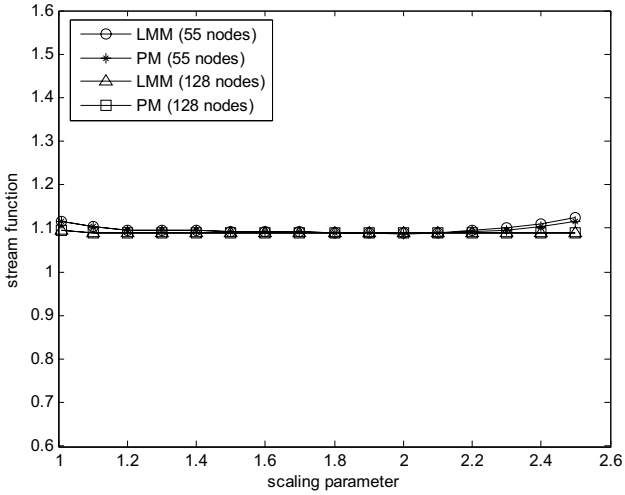

Fig. 3 Effect of scaling parameter on stream function (Ψ) at ($x = 4\ m, y = 1.5\ m$) for two sets of nodes

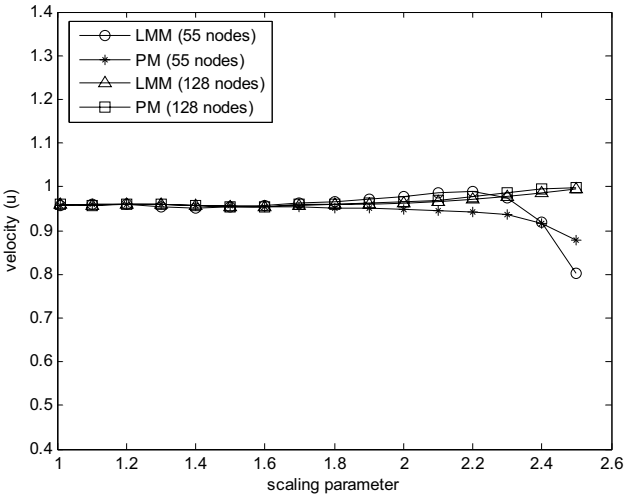

Fig. 4 Effect of scaling parameter on velocity (u) at ($x = 2\ m, y = 0.75\ m$) for two sets of nodes

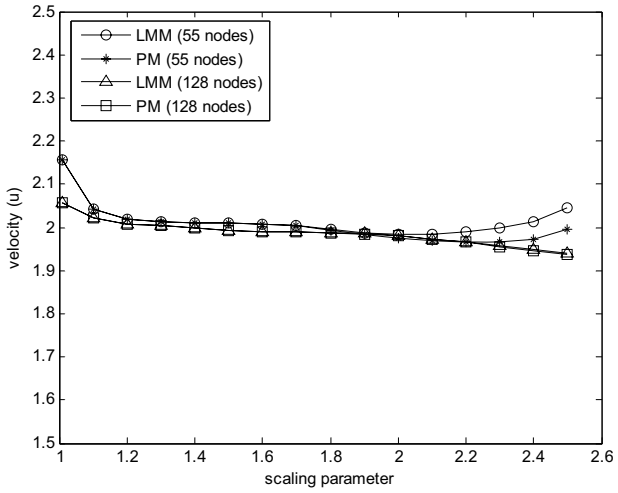

Fig. 5 Effect of scaling parameter on velocity (u) at ($x = 4\ m, y = 1.375\ m$) for two sets of nodes

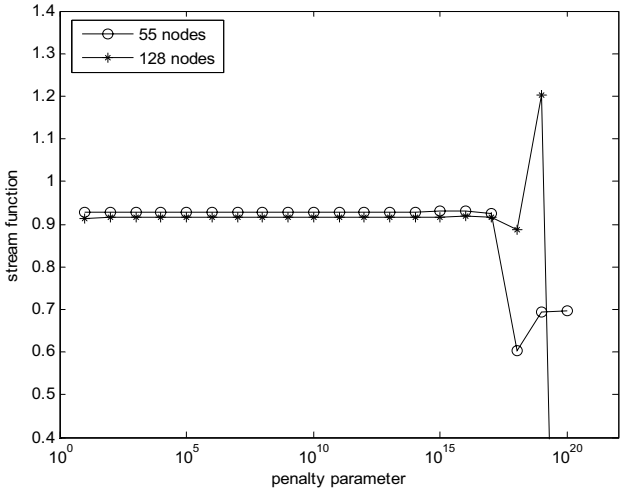

Fig. 6 Effect of penalty parameter on stream function (Ψ) at ($x = 2\ m, y = 1\ m$) for two sets of nodes

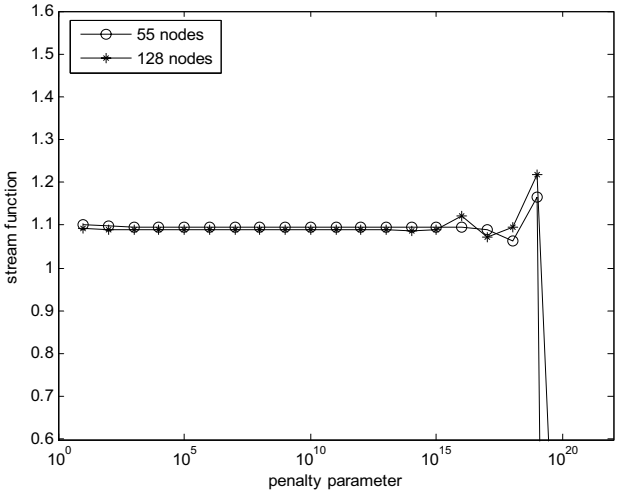

Fig. 7 Effect of penalty parameter on stream function (Ψ) at ($x = 4\ m, y = 1.5\ m$) for two sets of nodes

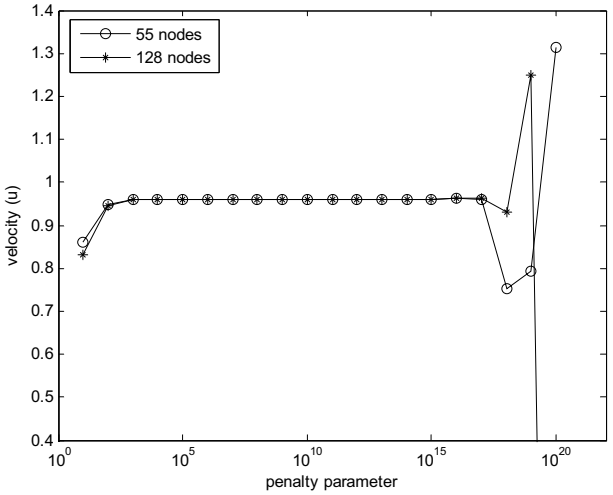

Fig. 8 Effect of penalty parameter on velocity (u) at ($x = 2\ m, y = 0.75\ m$) for two sets of nodes

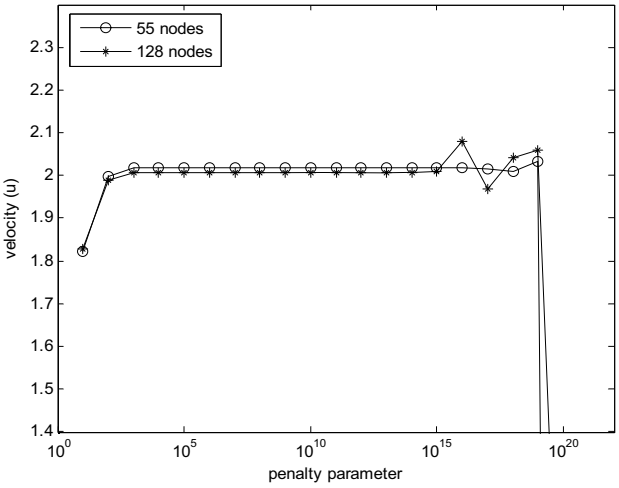

Fig. 9 Effect of penalty parameter on velocity (u) at ($x = 4\ m, y = 1.375\ m$) for two sets of nodes

B. Potential Flow over a Sphere

The model, data and its boundary conditions used for the potential flow over a sphere kept in cylinder are shown in Fig. 10. Lagrange multiplier and penalty methods have used to obtain the EFG results for two sets of nodes. Table 5 shows a comparison of stream function values (Ψ) obtained by EFG method with those obtained by FEM for 55 nodes at few typical locations. A similar comparison of EFG results with FEM is presented in Table 6 at the same locations for 128 nodes. The maximum percentage difference in stream function values obtained by LMM is found to be 0.81% for 55 nodes and 0.65% for 128 nodes, whereas the maximum percentage difference in stream function values obtained by PM is found to be 0.83% for 55 nodes and 0.65% for 128 nodes. A comparison of velocity values (u) obtained by EFG method with FEM is presented in Table 7 and Table 8 for 55 and 128 nodes respectively at the few typical locations. The maximum

percentage difference in velocity obtained by LMM is found to be 2.34% for 55 nodes and 0.66% for 128 nodes, whereas the maximum percentage difference in velocity values obtained by PM has been found to be 2.27% for 55 nodes and 0.66% for 128 nodes. From the results presented in Tables 5, 6, 7 & 8, it can be concluded that the results obtained by LMM are almost same as those obtained by PM. Moreover, with the increase in number of nodes, the EFG results start conversing for both LMM and PM.

The effect of scaling parameter ($d_{\max}$) on EFG results has been presented in Fig. 11 at the location ($x = 2, y = 1$) for 55 and 128 nodes. A similar comparison of EFG results has been presented in Fig. 12 at ($x = 4, y = 1.5$), in Fig. 13 at ($x = 2, y = 0.75$) and in Fig. 14 at ($x = 4, y = 1.5$) for the same set of sets. From the results presented in Figs. 11─14, it has been observed that the scaling parameter gives acceptable results in the range 1.2─1.8 for both LMM and PM.

The effect of penalty parameter (α) on EFG results has been presented in Fig. 15 at the location ($x = 2, y = 1$) for 55 and 128 nodes. A similar comparison of EFG results has been presented in Figs. 16, 17 and 18 at the locations ($x = 4, y = 1.5$), ($x = 2, y = 0.75$) and ($x = 4, y = 1.5$) respectively for 55 and 128 nodes. From Figs. 15─18, it has been noticed that the acceptable range of penalty parameter varies from 10^3 to 10^{16}.

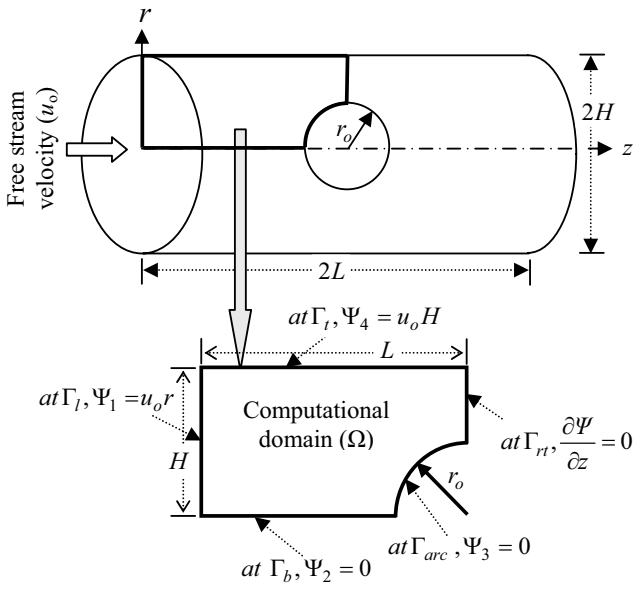

($L = 4$ m, $H = 2$ m, $r_o = 1$ m, $u_o = 1$m/s)

Fig. 10 Potential flow over a sphere kept inside the cylinder

TABLE V COMPARISON OF STREAM FUNCTION (Ψ) WITH FEM FOR 55 NODES AT THE FEW TYPICAL LOCATIONS

Location		55 nodes				
		EFG				FEM
x	y	LMM	% diff	PM	% diff	
1.0	1.5	1.1938	0.16	1.1936	0.14	1.1919
1.5	1.5	1.1465	0.16	1.1463	0.14	1.1447
2.0	1.5	1.1169	0.13	1.1167	0.12	1.1154
3.0	1.5	1.0178	0.20	1.0178	0.20	1.0158
3.0	1.0	0.3443	0.55	0.3443	0.55	0.3462
4.0	1.75	1.4152	0.13	1.4150	0.14	1.4170
4.0	1.5	0.8989	0.19	0.8988	0.18	0.8972
4.0	1.25	0.4299	0.81	0.4298	0.83	0.4334

TABLE VI COMPARISON OF STREAM FUNCTION (Ψ) WITH FEM FOR 128 NODES AT THE FEW TYPICAL LOCATIONS

Location		128 nodes				
		EFG				FEM
x	y	LMM	% diff	PM	% diff	
1.0	1.5	1.2028	0.06	1.2026	0.04	1.2021
1.5	1.5	1.1565	0.04	1.1562	0.02	1.1560
2.0	1.5	1.1266	0.06	1.1264	0.04	1.1259
3.0	1.5	1.0248	0.03	1.0247	0.02	1.0245
3.0	1.0	0.3548	0.50	0.3548	0.50	0.3566
4.0	1.75	1.4145	0.03	1.4144	0.04	1.4149
4.0	1.5	0.8947	0.11	0.8946	0.12	0.8957
4.0	1.25	0.4280	0.65	0.4280	0.65	0.4308

TABLEVII COMPARISON OF VELOCITY (u) WITH FEM FOR 55 NODES AT THE FEW TYPICAL LOCATIONS

Location		55 nodes				
		EFG				FEM
x	y	LMM	% diff	PM	% diff	
1.5	1.75	0.9756	0.18	0.9756	0.18	0.9774
1.5	0.75	1.0325	0.15	1.0323	0.13	1.0310
3.0	1.25	1.0776	0.59	1.0776	0.59	1.0713
3.0	0.75	0.8290	2.34	0.8296	2.27	0.8489
4.0	1.875	1.2476	0.32	1.2480	0.35	1.2436
4.0	1.625	1.2708	0.70	1.2706	0.71	1.2797
4.0	1.375	1.3644	1.13	1.3644	1.13	1.3492
4.0	1.125	1.5285	0.80	1.5282	0.82	1.5409

TABLE VIII COMPARISON OF VELOCITY (u) WITH FEM FOR 128 NODES AT THE FEW TYPICAL LOCATIONS

Location		128 nodes				
		EFG				FEM
x	y	LMM	% diff	PM	% diff	
1.5	1.75	0.9643	0.03	0.9643	0.03	0.9646
1.5	0.75	1.0123	0.03	1.0120	0.00	1.0120
3.0	1.25	1.0720	0.30	1.0718	0.28	1.0688
3.0	0.75	0.8504	0.24	0.8504	0.24	0.8484
4.0	1.875	1.2491	0.08	1.2493	0.10	1.2481
4.0	1.625	1.2795	0.10	1.2795	0.10	1.2782
4.0	1.375	1.3576	0.40	1.3573	0.38	1.3522
4.0	1.125	1.5218	0.66	1.5218	0.66	1.5319

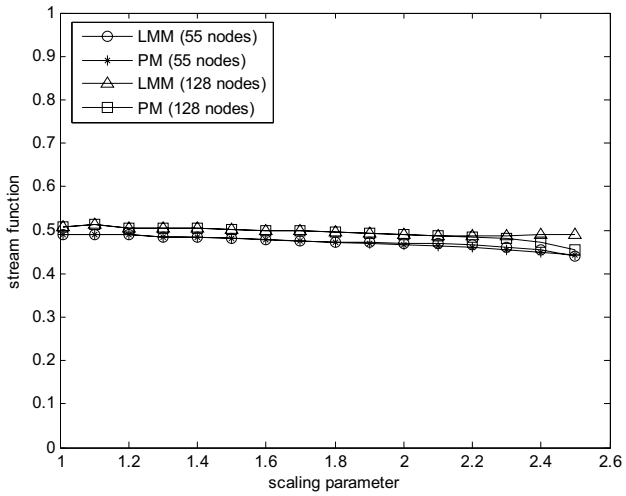

Fig. 11 Effect of scaling parameter on stream function (Ψ) at ($x = 2\ m, y = 1\ m$) for two sets of nodes

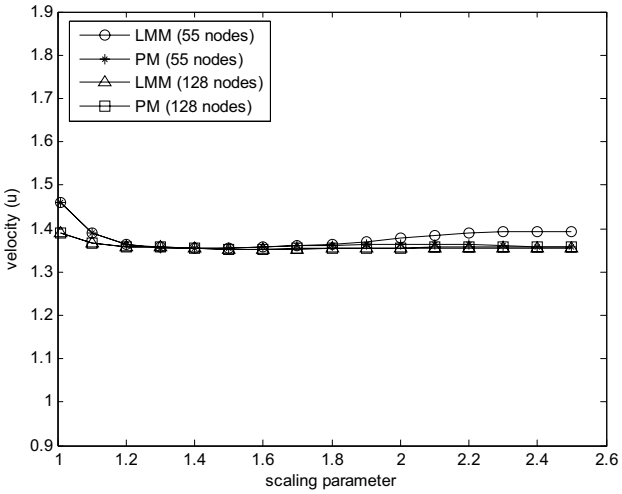

Fig. 14 Effect of scaling parameter on velocity (u) at ($x = 4\ m, y = 1.5\ m$) for two sets of nodes

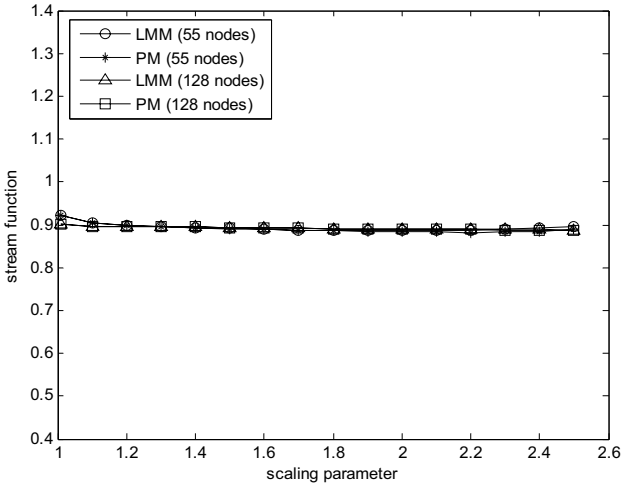

Fig. 12 Effect of scaling parameter on stream function (Ψ) at ($x = 4\ m, y = 1.5\ m$) for two sets of nodes

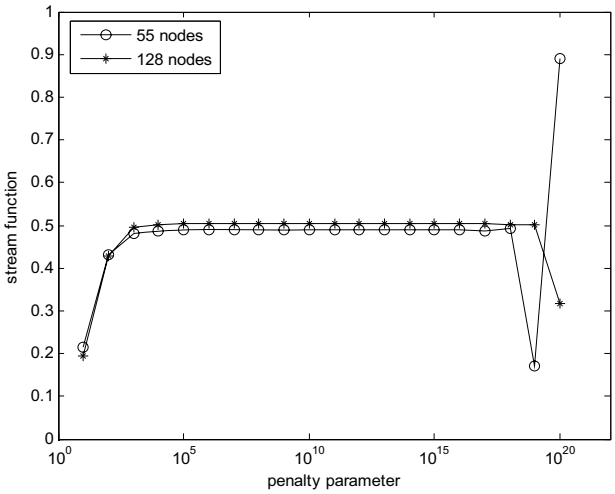

Fig. 15 Effect of penalty parameter on stream function (Ψ) at ($x = 2\ m, y = 1\ m$) for two sets of nodes

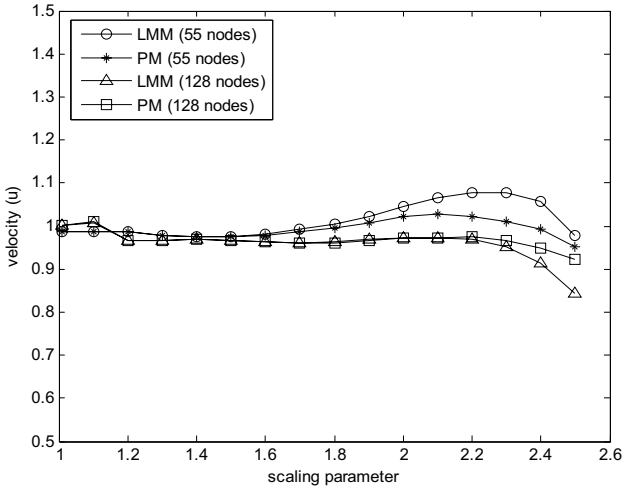

Fig. 13 Effect of scaling parameter on velocity (u) at ($x = 2\ m, y = 0.75\ m$) for two sets of nodes

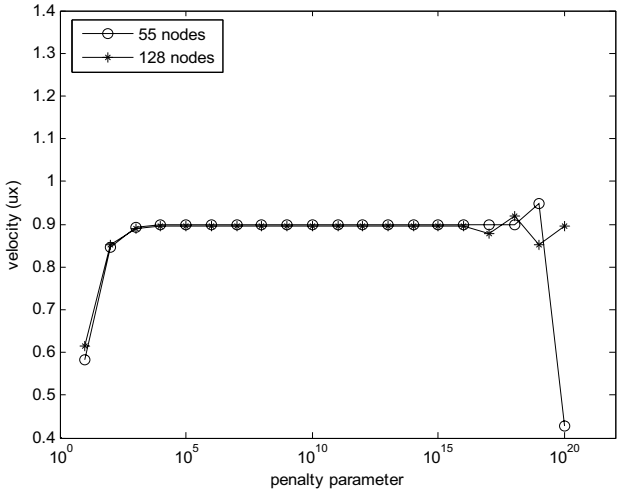

Fig. 16 Effect of penalty parameter on stream function (Ψ) at ($x = 4\ m, y = 1.5\ m$) for two sets of nodes

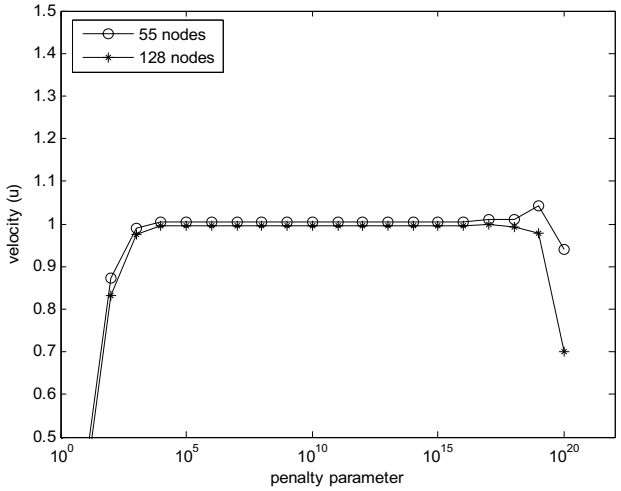

Fig. 17 Effect of penalty parameter on velocity (u) at ($x = 2\ m, y = 0.75\ m$) for two sets of nodes

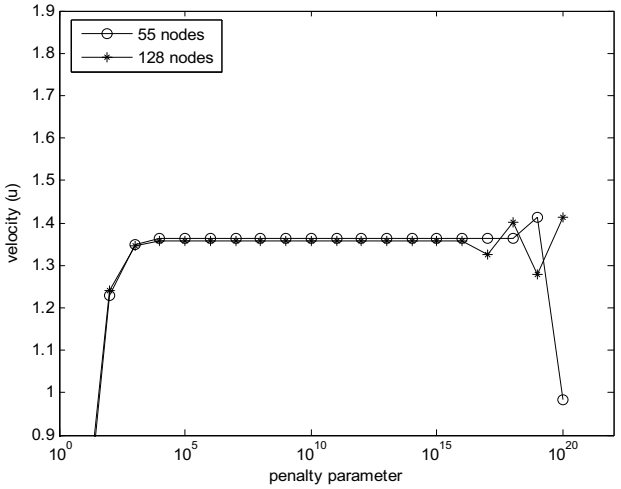

Fig. 18 Effect of penalty parameter on velocity (u) at ($x = 4\ m, y = 1.5\ m$) for two sets of nodes

VI. Conclusions

In this paper, meshless element free Galerkin method has been successfully extended to solve two-dimensional potential flow problems. The essential boundary conditions were enforced using penalty and Lagrange multiplier techniques. Four point Gauss quadrature were used to evaluate the integrals over the two-dimensional domain and nodal integration scheme was used for the application of essential boundary conditions on the edges. The meshless numerical results have been obtained for a sample data and are compared with those obtained by finite element method. It was noticed that the results obtained by EFG method have been found in good agreement with those obtained by finite element method. Moreover, with the increase in number of nodes EFG results start conversing for both Lagrange multiplier and penalty methods. From above analysis, it was also noticed that the results obtained by Lagrange multiplier and penalty methods are almost similar for potential flow problems. The range of scaling ($d_{\max}$) and penalty (α) parameters has been found to be $1.2 \le d_{\max} \le 1.8$ and $10^3 \le \alpha \le 10^{15}$ respectively. Finally it can be concluded that the penalty method can be used in fluid flow problems due to its simplicity in applying the essential boundary conditions.

Notations

$a_j(\mathbf{x})$ = non constant coefficients

% diff = percentage difference of EFG results with FEM

H = height of computational domain

L = Length of computational domain

m = number of terms in the basis

n = number of nodes in the domain of influence

N_{K} = Lagrange interpolant

$p_j(\mathbf{x})$ = monomial basis function

$\bar{r}$ = normalized radius

r_o = radius of sphere/cylinder

u = x -component of velocity

$w(\mathbf{x} - \mathbf{x}_I)$ = weight function used in MLS approximation

w_1 = weighting function used in weighted integral form

α = penalty parameter

$\lambda_1, \lambda_2, \lambda_3 \text{ and } \lambda_4$ = Lagrange multipliers

Γ = boundary of the computational domain

Ω = two-dimensional computational domain

Ψ = stream function

$\Psi^h(\mathbf{x})$ = approximation function for stream function

$\Phi_I(\mathbf{x})$ = shape function

References

[1] H. Lin, and S. N. Atluri, "The meshless local Petrov Galerkin (MLPG) method for solving incompressible Navier-Strokes equation," *Comp. Modeling Eng. Sci*., vol. 2, pp. 117-142, 2001.

[2] H. Lin, and S. N. Atluri, "Meshless local Petrov Galerkin (MLPG) method for convection-diffusion Problems," *Comp. Modeling Eng. Sci.,* vol. 1, pp. 45-60, 2000.

[3] E. Oňate, and S. Idelsohn, "A mesh-free point method for advective-diffusive transport and fluid flow problems," *Comput. Methods*, vol. 21, pp. 283-292, 1998.

[4] E. Oňate, S. Idelsohn, O. C. Zienkiewicz, R. L. Taylor, and C. Sacco, "A stabilized finite point method for analysis of fluid mechanics problems," *Comp. Methods Appl. Mech. Eng.*, vol. 139, pp. 315-346, 1996.

[5] R. Löhner, C. Sacco, E. Oňate, and S. Idelsohn, "A finite point method for compressible flow," *Int. J. Numer. Methods Eng.,* vol. 53, pp. 1765-1779, 2002.

[6] T. Sophy, and H. Sadat, "A meshless formulation for three dimensional laminar natural convection," *Numer. Heat Transfer*, vol. 41, pp. 433-445, 2002.

[7] W. K. Liu, S. Jun, D. T. Sihling, Y. Chen, and W. Hao, "Multiresolution reproducing kernel paticle method for computational fluid dynamics," *Int. J. Numer. Methods Fluids,* vol. 24, pp. 1391-1415, 1997.

[8] Y. C. Hon, S. Li, and M. Huang, "A meshless computational method for the shear flow of Johnson-Segalman fluid," *Int. J. Comput. Methods Eng. Mech.,* vol. 6, pp. 59-64, 2005.
[9] I. Tsukanov, V. Shapiro, and S. Zhang, "A meshfree method for incompressible fluid dynamics problems," *Int. J. Numer. Methods Eng.*, 58, pp. 127-158, 2003.
[10] T. Chen, and I. S. Raju, "A coupled finite element and meshless local Petrov-Galerkin method for two-dimensional potential problems," *Comp. Methods Appl. Mech. Eng.*, vol. 192, pp. 4533-4550, 2003.
[11] M. Cheng, and G. R. Liu, "A noval finite point method for flow simulation," *Int. J. Numer. Methods Fluids,* vol. 39, pp. 1161-1178, 2002.
[12] I. V. Singh, "Application of meshless EFG method in fluid flow problems," *Sadhana,* vol. 29, pp. 285-296, 2004.
[13] C. Du, "An element free Galerkin method for simulation of stationary two-dimensional shallow water flows in river," *Comp. Methods Appl. Mech. Eng.*, vol. 182, pp. 89-107, 2000.
[14] S. L. L. Veradi, J. M. Machado, and J. R. Cardoso, "The element-free Galerkin method applied to the study of fully developed magnetohydrodynamic duct flows," *IEEE Trans. Magnetics,* vol. 38*,* pp. 941-944, 2002.
[15] I. V. Singh, K. Sandeep, and R. Prakash, "Heat transfer analysis of two-dimensional fins using meshless element-free Galerkin method," *Numer. Heat Transfer*, vol. 44, pp. 73-84, 2003.
[16] T. J. Chung, *Finite Element Analysis in Fluid Dynamics*, McGraw-Hill: USA, 1978, pp. 170-202.